ISSN 0027-1349, Moscow University Physics Bulletin, 2023, Vol. 78, No. 2, pp. 173–178. © Allerton Press, Inc., 2023.
ISSN 0027-1349, Moscow University Physics Bulletin, © 2023, Allerton Press, Inc., 2023.

OPTICS AND SPECTROSCOPY. LASER PHYSICS

Finite Voxel Size Compensation for Microprinting of Parabolic X-ray Lenses by Two-Photon Lithography

M. I. Sharipova[1*], T. G. Baluyan[1], A. S. Sverchkov[1], D. A. Shilkin[1], V. O. Bessonov[1], and A. A. Fedyanin[1]

[1]*Department of Nanophotonics, Faculty of Physics, Lomonosov Moscow State University, Moscow, 119991 Russia*

Received September 29, 2022; revised December 8, 2022; accepted December 12, 2022

Abstract—Three-dimensional microprinting by two-photon laser lithography is a promising way to manufacture X-ray lenses. However, as the radius of curvature approaches the voxel size, the refractive surface of the lens deviates from the specified shape, that leads to a deterioration in the focusing of X-ray radiation and astigmatism. In this work we suggest a method for correcting a model for 3D printing of a parabolic X-ray lens taking into account the finite voxel size.

Keywords: two-photon lithography, voxel, X-ray lenses

DOI: 10.3103/S0027134923020091

INTRODUCTION

X-rays have numerous applications in science and technology due to the possibility of observing diffraction on crystal lattices, low reflection coefficient when passing through interfaces, and ionizing properties [1]. One of the actively developing applications of this radiation is X-ray microscopy [2–5]. For its further development, the creation of lenses capable of focusing X-rays on the microscopic scale with minimal aberrations is in particular demand.

The refractive index n in medium for X-ray spectral range can be expressed as $n = 1 - \delta + i\beta$, where δ is the decrement of the refractive index and β is the imaginary part of the refractive index responsible for absorption. The characteristic values of δ range from 10^{-5} to 10^{-7}, and β—from 10^{-6} to 10^{-8} [6]. Small value of δ leads to a weak optical power of a single X-ray lens: for example, an aluminium lens with a 300 μm radius of curvature focuses the X-ray radiation with an energy of 14 keV at a distance of 54 m [7]. To reduce the focal length, several single lenses are arranged coaxially to form a compound X-ray refractive lens (CRL). In thin lens approximation, the focal length of the CRL is $f = R/2N\delta$ [8], where R is the radius of curvature of the refractive surfaces of the lens near the optical axis, and N is the number of identical single lenses in the CRL. To further reduce the focal length f, the radius of curvature R is set to small values ranging from units [9] to hundreds of micrometers [10]. The optimal refracting surface for focusing synchrotron X-rays is a Cartesian oval [11]. Near the optical axis, this shape is approximated to a high degree of accuracy by a parabola, and in the three-dimensional case, the ideal refracting surface is close to a paraboloid formed by the rotation of a parabola around the optical axis. The optimal configuration of the CRL is therefore an array of coaxially arranged concave parabolic surfaces with a radius of curvature of about a few micrometers at the apex. The focusing of X-ray radiation by an ideal CRL is shown schematically in Fig. 1a.

Recently the two-photon lithography (TPL) method has been shown to be well suited for the fabrication of CRLs [12]. TPL is a modern method for printing three-dimensional micro-objects out of photocurable polymers (photoresists). TPL has been successfully used to fabricate optical waveguides [13], microlenses [14], biocompatible microparticles [15], metamaterials [16] and metasurfaces [17], photonic crystals [18–20], composite structures [21], and elements of refractive X-ray optics [12, 22]. The TPL method allows to fabricate optically smooth three-dimensional microstructures [23] of arbitrary design with a resolution down to 100 nm [24] and to position them relative to each other with submicron accuracy [25]. Therefore, TPL is suitable for fabrication of both CRL with a small radius of curvature [22, 26],

*E-mail: sharipova@nanolab.phys.msu.ru

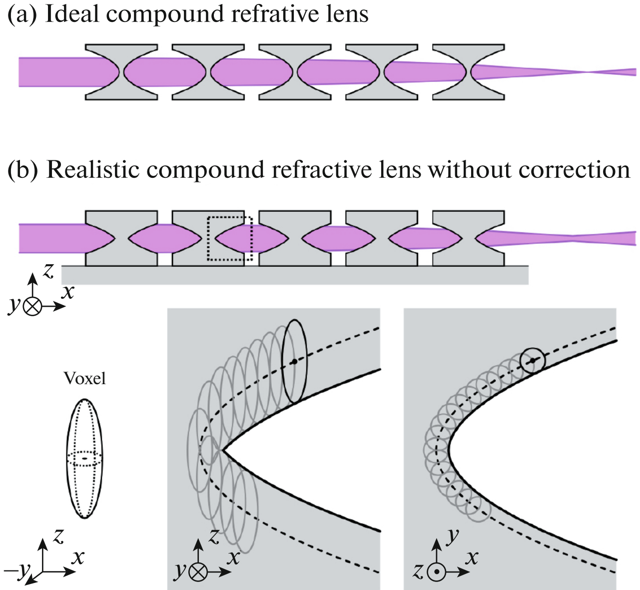

Fig. 1. Schematic representation of (a) ideal and (b) realistic CRLs, where the latter is fabricated by two-photon lithography without finite voxel size correction. The voxel shape and its trajectories during CRL fabrication in both vertical and horizontal cross-sections are shown below.

and of other optical elements [27, 28] and complex optical systems [29].

It has been previously demonstrated [30] that parabolic lenses fabricated by the TPL method focus X-ray radiation with astigmatism: the minimum sizes of the focal spot in the horizontal and vertical cross-sections are observed at different focal distances. The astigmatism is caused by the fact that the lenses produced by the TPL method lack rotational symmetry relative the optical axis, which in turn can be explained by the different print resolution along different directions. The TPL printing process is the movement of a focused laser beam, which causes polymerization of the photoresist in the region of the focal point. The minimal unit of polymerizable volume, which is named a voxel, is typically shaped as an ellipsoid of revolution extended along the axis of laser radiation propagation [31].

The characteristic sizes of the ellipsoid axes are typically fractions of a micrometer in the transverse direction and on the order of a micrometer in the direction of laser radiation propagation [32, 33]. For example, in [30] the voxel sizes across and along the axis of laser radiation propagation were estimated to be 0.6 and 1 μm, respectively. The radius of curvature of the manufactured lenses was $R = 5$ μm, which is comparable to the voxel dimensions. As the absorbed radiation dose increases, i.e., as the laser power increases or the printing speed decreases, the ratio of the axial to lateral voxel dimensions increases [34].

Figure 1b shows the focusing of the radiation using a realistic CRL produced by the TPL method; the process of the CRL fabrication without correction for the final voxel size is also schematically shown. The laser beam travels along the trajectories of a given three-dimensional model corresponding to the surface of a paraboloid of revolution. The paraboloid's curvature radius R is comparable to the voxel size. The resulting surface of the fabricated lens is an envelope for a family of elongated ellipsoidal voxels, whose centers lie on the surface of the paraboloid of revolution. The elongated voxel shape leads to the difference in the horizontal and vertical cross-sections of this envelope when the lens optical axis does not coincide with the ellipsoidal axis of symmetry, as it is shown in Fig. 1b. The asymmetry of the manufactured lens results in astigmatism. However, if the lens is printed in a vertical geometry, i.e., when the laser light propagation direction, and thus the voxel symmetry axis, is aligned with the optical axis of the lens, its refractive surface remains symmetric and astigmatism is absent [22]. The vertical geometry in TPL process is preferable for fabrication astigmatism-free lenses, but using this configuration it is technically difficult to make CRLs from a large number of lenses due to the high aspect ratio. In addition, in the case of vertically oriented CRL, X-rays have to pass through the substrate and are therefore partially absorbed. In addition, even though a CRL produced by TPL in vertical geometry has cylindrical symmetry, the refractive surface of the lens (the envelope for the family of voxel surfaces with moving center) still deviates from the parabolic shape, causing aberrations.

In this paper we solve the problem of correcting a parabolic lens model for its printing by two-photon lithography taking into account the finite voxel size.

1. ANALYTICAL EXPRESSION FOR THE CORRECTED CRL MODEL

1.1. Two-Dimensional Case

The geometry of the problem in the two-dimensional case is shown in Fig. 2a.

Let us write the equation of the target parabola in the following form:

$$z^2 = 2Rx, \tag{1}$$

where R is the parabola's radius of curvature at the origin of the coordinates.

We can use the ellipse equation for the voxel surface:

$$\frac{(x - x_c)^2}{a^2} + \frac{(z - z_c)^2}{b^2} = 1, \tag{2}$$

where a, b are semi-axes, and we assume that $a/b < 1$, (x_c, z_c) are coordinates of the ellipse center. As the

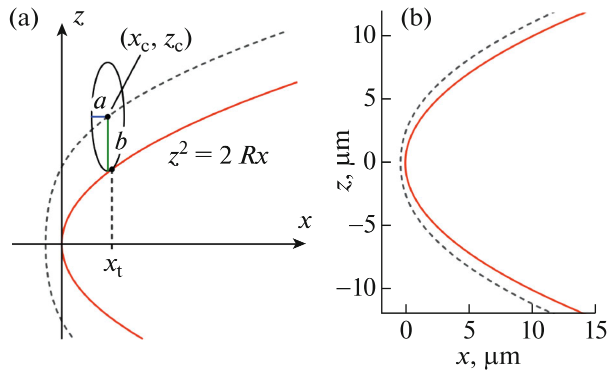

Fig. 2. Analytical approach. (a) The geometry of the problem. (b) Solution for the experimental parameters. The target parabola is shown as a continuous curve, the voxel trajectory—as a dashed curve.

voxel center moves along the desired trajectory, the boundary curve of the area covered by voxels should form the target parabola. To do this, each voxel should touch the parabola at each voxel position, i.e., moving voxel must have a common point and a common tangent with the parabola for the whole set of values (x_c, z_c). By equating the derivatives dz/dx for the equation of the parabola (1) and the equation of the ellipse (2), after transformations we can express voxel center coordinate x_c through the tangent point coordinate x_t:

$$x_c\,(x_t) = x_t - \frac{a^2}{\sqrt{a^2 + 2b^2 x_t/R}}. \qquad (3)$$

Using the ellipse equation (2) and setting $x = x_t$, $z = \pm\sqrt{2Rx_t}$, for the second coordinate of the voxel center we have the following expression:

$$z_c\,(x_t) = \pm\sqrt{x_t}\left[\sqrt{2R} + \frac{2b^2}{\sqrt{2Ra^2 + (2b)^2 x_t}}\right]. \qquad (4)$$

Expressions (3) and (4) parametrically define the trajectory of the ellipse center, and the boundary of the area covered by the moving ellipse is the target parabola. The dashed curve in Fig. 2b shows the solution for parameters $a = 0.375$ μm, $b = 1.075$ μm, and $R = 5$ μm, while the continuous red curve designates the target parabola. The selected values of the elliptical voxel semi-axes a and b correspond to the characteristic values in TPL printing; the R value corresponds to the previously produced CRLs with astigmatism [30]. Due to the elongated shape of the voxel, the distance between its center trajectory and the target parabola is minimal near the top of the parabola and increases with distance from the optical axis.

1.2. Thee-Dimensional Case

For the practical case of the correction problem, the three-dimensional case is relevant, in which the equation for the desired shape of the lens in the form of a paraboloid of revolution has the following form:

$$2Rx = y^2 + z^2. \qquad (5)$$

The equation of an ellipsoid of revolution can be used to describe the voxel shape:

$$\frac{(x - x_c)^2}{a^2} + \frac{(y - y_c)^2}{a^2} + \frac{(z - z_c)^2}{b^2} = 1. \qquad (6)$$

Qualitatively, the problem is similar with the two-dimensional case: when an elliptic voxel moves along the desired surface, the boundary surface of the volume swept by the voxel must be a paraboloid of revolution. To satisfy this condition, the voxel should touch the paraboloid at its each point and have a common tangent plane with it. Equating the tangent planes for the paraboloid and the ellipsoid at the tangent point $\mathrm{T}(x_t, y_t, z_t)$, after transformations we have the following expressions:

$$\begin{cases} 2Rx_t = y_t^2 + z_t^2, \\[2ex] \dfrac{(x_t - x_c)^2}{a^2} + \dfrac{(y_t - y_c)^2}{a^2} + \dfrac{(z_t - z_c)^2}{b^2} = 1, \\[2ex] \dfrac{-R}{x_t - x_c} = \dfrac{y_t}{y_t - y_c} = \dfrac{z_t}{(z_t - z_c)a^2/b^2}. \end{cases} \qquad (7)$$

From that we can obtain parametric equations for the voxel center coordinate as a function of the tangent point (x_t, y_t, z_t):

$$\begin{cases} x_c = x_t - \dfrac{aR}{\sqrt{R^2 + y_t^2 + \dfrac{b^2}{a^2} z_t^2}}, \\[3ex] y_c = y_t\left(1 + \dfrac{a}{\sqrt{R^2 + y_t^2 + \dfrac{b^2}{a^2} z_t^2}}\right), \\[3ex] z_c = z_t\left(1 + \dfrac{b^2}{a^2}\dfrac{a}{\sqrt{R^2 + y_t^2 + \dfrac{b^2}{a^2} z_t^2}}\right). \end{cases} \qquad (8)$$

Expressions (8) were used to construct a corrected three-dimensional model of the parabolic X-ray lens shown in Fig. 3, for voxel parameters $a = 0.375$ μm and $b = 1.075$ μm.

We have used the following geometric parameters of the lens, which are comparable to the size of lenses used in synchrotron experiments [30]: entrance aperture $A = 28$ μm, radius of curvature at the apex of the

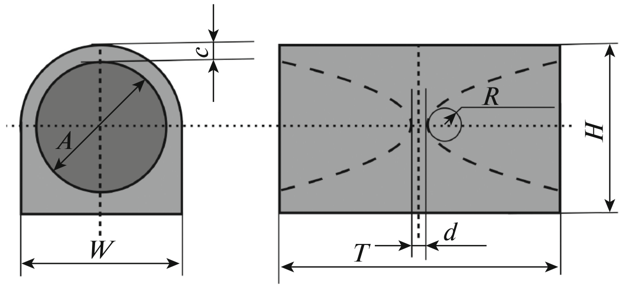

Fig. 3. Schematic of a parabolic X-ray lens with finite voxel size correction.

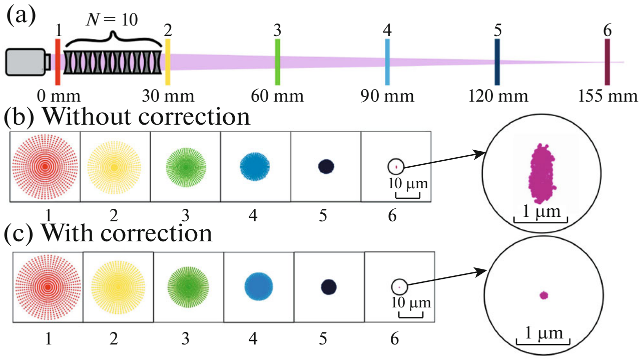

Fig. 4. Numerical simulations. (a) The geometry of the optical system. The vertical color lines indicate the distances at which the cross sections of the optical beam were registered. (b) Cross-sections of the optical beam passing through the CRL without correction for voxel size. (c) Cross-sections of the optical beam passing through the CRL with correction.

parabolas $R = 5\ \mu$m, lens rim size $c = 2\ \mu$m, distance between the apexes of parabolic refractive surfaces $d = 1\ \mu$m, length $T = 40.2\ \mu$m.

2. NUMERICAL SIMULATION OF X-RAY FOCUSING USING CRLs WITH AND WITHOUT CORRECTION

To perform the numerical simulation of the X-ray focusing by the CRL, we have used the ray tracing method in the Comsol Multiphysics software package. A cylindrical grid with 15 radial and 60 angular positions was used to simulate the beam of synchrotron radiation falling on the CRL, and a total of 900 beams were included in the simulations. The beam diameter corresponded to the diameter of the entrance aperture of the lens.

Figure 4a shows a schematic of the numerical experiment: a source emits a beam of monochromatic X-ray radiation in a vacuum with a wavelength of 1 Å, which passes through a CRL consisting of 10 coaxial parabolic lenses, with a distance of 100 μm between the centers of neighboring lenses.

The following values of optical constants were used: $\delta = 1.614 \times 10^{-6}$, $\beta = 1.917 \times 10^{-8}$, which correspond to parameters for commercially available polymer SZ2080 [35] commonly used in the manufacture of TPL structures. Two variants of the CRL were used in modeling: the first CRL consists of individual lenses without correction and the second uses lenses with voxel correction. In the first case, a three-dimensional mesh corresponding to the envelope surface for a family of elongated ellipsoidal voxels whose centers are located on the surface of a paraboloid of rotation was computed numerically in the Python software to create a lens without correction. The obtained values were processed using MeshLab and Autodesk 3DsMax software, resulting in the simulation of a three-dimensional microlens of a non-ideal shape in stl format, imitating lens fabrication by the TPL method without regard to the finite voxel size. In the second version, the CRL consists of lenses with ideal parabolic refractive surfaces corresponding to TPL lens fabrication with finite voxel size compensation.

Figure 4b shows X-ray beam cross sections perpendicular to the direction of radiation propagation when passing through the CRL without correction. At the entrance to the CRL (0 mm), the X-rays fill a circle with a diameter of 28 μm. After the CRL, the transverse dimensions of the beam decrease, but this occurs in a non-uniform manner. At a distance of $L =$ 120 mm (blue circles) the cross section is flattened in the vertical direction. At the calculated focal distance $L = 155$ mm (purple circles), the focal spot changes shape, extending along the vertical direction. The enlarged cross section of the X-ray beam at distance $L = 155$ mm is shown in the circular inset on the right (Fig. 4b). Since the uncorrected lens surface has no rotational symmetry with respect to the optical axis, it refracts light unequally in the vertical and horizontal directions. This results in astigmatism and pronounced asymmetry of the focal spot. In the second case of a corrected CRL, the sections of the X-ray beam have the same circular shape (Fig. 4c), which does not depend on the distance to the CRL. At a distance of $L = 155$ mm (in the circular inset on the right, Fig. 4c), the focal spot is smaller for the corrected CRL than for the uncorrected CRL.

This effect is clearly shown in Fig. 5, where the dependence of the beam size D in the horizontal and vertical sections on the distance L to the entrance aperture of the CRL is plotted for CRLs without correction (green triangles—vertical section, red squares—horizontal section) and with correction (blue circles for both sections).

The black curve shows the dependence obtained analytically for an ideal lens according to the expression $D = A\,|L/f - 1|$. There is astigmatism for uncorrected CRL: the focal lengths for the vertical and

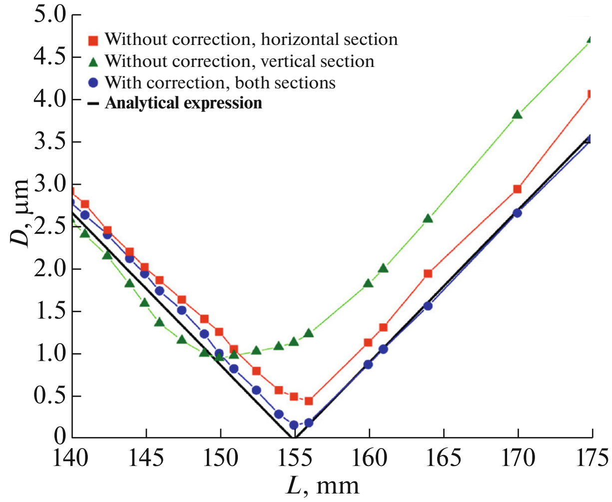

Fig. 5. Beam section size D as a function of the distance to the CRL inlet aperture L. For the model without correction beam sizes in horizontal and vertical cross-sections are shown by red squares and green triangles, respectively. For model with correction blue circles denote beam size for both cross-sections. The black curve shows the analytically obtained dependence for an ideal CRL.

horizontal sections of the X-ray beam are different. The meridional and sagittal focal lengths are $F_v = 150$ mm and $F_h = 156$ mm, respectively. The difference in focal lengths $\Delta F = |F_v - F_h|$ is 6 mm, which is similar to the value obtained in previous experimental work [30]. The beam waist size in the vertical cross-section is 970 nm, while in the horizontal cross-section it equals 460 nm, approximately twice smaller. In [22], different beam sizes were observed in the vertical and horizontal sections, with a ratio of values of approximately 1.5, which can be explained by different values of key parameters, such as radius of curvature at the lens apex R and voxel's semi-axes ratio a/b.

In the case of CRL with correction, the astigmatism disappears: the minimum beam size is observed at 155 mm from the CRL for both vertical and horizontal beam sections. The focal spot is a circle of 180 nm diameter. The finite size of the focal spot can be explained by calculation error and the difference of the refracting surface from the Cartesian oval, but this value already lies beyond the diffraction limit, which value has been calculated to be 415 nm for this system [36].

Although diffraction is not taken into account in this simulation, the exploited calculation method shows that, by correcting the lens model for voxel size, astigmatism can be avoided and a smaller symmetrical focal spot can be achieved.

CONCLUSIONS

To conclude, in this work we have presented an analytical expression for the correction of an X-ray lens model with a parabolic profile that takes into account the finite voxel size when printed by two-photon laser lithography. The proposed method based on the finite voxel size compensation avoids the astigmatism of X-ray lenses manufactured by two-photon lithography. In addition, the size of the beam waist in the vertical section is reduced from 970 to 180 nm, and in the horizontal section—from 460 to 180 nm. The proposed correction will make it possible to develop the application of two-photon laser lithography for manufacturing refractive synchrotron X-ray optical elements and to increase the resolution in X-ray microscopy.

FUNDING

The research was carried out with support from the Interdisciplinary Scientific and Educational School of Moscow University "Photonic and Quantum Technologies. Digital Medicine." The research was supported by the Ministry of Science and Higher Education of the Russian Federation (grant no. 075-15-2021-1353).

CONFLICT OF INTEREST

The authors declare that they have no conflicts of interest.

REFERENCES

1. J. G. Brown, *X-rays and Their Applications* (Springer, New York, 2012).
2. B. Niemann, D. Rudolph, and G. Schmahl, Appl. Opt. **15**, 1183 (1976). https://doi.org/10.1364/AO.15.001883
3. P. Kirkpatrick and A. V. Baez, J. Opt. Soc. Am. **38**, 766 (1948). https://doi.org/10.1364/JOSA.38.000766
4. J. Kirz and C. Jacobsen, J. Phys.: Conf. Ser. **186** (2009). https://doi.org/10.1088/1742-6596/186/1/012001
5. M. I. Mazuritskiy and A. M. Lerer, JETP Letters **112**, 138 (2020). https://doi.org/10.1134/S0021364020150072
6. D. Serebrennikov, E. Clementyev, A. Semenov, and A. Snigirev, J. Synchrotron Radiat. **23**, 1315 (2016). https://doi.org/10.1107/S1600577516014508
7. A. Snigirev, V. Kohn, I. Snigireva, and B. Lengeler, Nature **384**, 49 (1996). https://doi.org/10.1038/384049a0
8. B. Lengeler, C. Schroer, J. Tümmler, et al., J. Synchrotron Radiat. **6**, 1153 (1999). https://doi.org/10.1107/S0909049599009747

9. M. Lyubomirskiy, I. Snigireva, V. Kohn, et al., J. Synchrotron Radiat. **23**, 1104 (2016). https://doi.org/10.1107/S160057751601153X
10. R. Celestre, S. Antipov, and E. Gomez, J. Synchrotron Radiat. **29**, 629 (2022). https://doi.org/10.1107/S1600577522001795
11. M. Sanchez del Rio and L. Alianelli, J. Synchrotron Radiat. **19**, 366 (2012). https://doi.org/10.1107/S0909049512003020
12. A. K. Petrov, V. O. Bessonov, K. A. Abrashitova, et al., Opt. Express **25**, 14173 (2017). https://doi.org/10.1364/OE.25.014173
13. K. R. Safronov, D. N. Gulkin, I. M. Antropov, et al., ACS Nano **14**, 10428 (2020). https://doi.org/10.1021/acsnano.0c04301
14. T. Gissibl, S. Thiele, A. Herkommer, and H. Giessen, Nature Photon. **10**, 554 (2016). https://doi.org/10.1038/nphoton.2016.121
15. J. Serbin, A. Egbert, A. Ostendorf, et al., Opt. Lett. **28**, 301 (2003). https://doi.org/10.1364/OL.28.000301
16. T. Bückmann, N. Stenger, and M. Kadic, Mater. **24**, 2710 (2012). https://doi.org/10.1002/adma.201200584
17. H. Yang, Ch. Wang, Proc. of SPIE **11850**, 118500K (2021). https://doi.org/10.1117/12.2599414
18. I. Shishkin, K. Samusev, M. Rybin, M. Limonov, Yu. Kivshar, A. Gaidukeviciute, R. Kiyan, and B. Chichkov, JETP Letters **95**, 457 (2012). https://doi.org/10.1134/S0021364012090123
19. I. I. Shishkin, M. V. Rybin, K. B. Samusev, M. V. Limonov, R. V. Kiyan, B. N. Chichkov, Yu. S. Kivshar, and P. A. Belov, JETP Letters **99**, 531–534 (2014). https://doi.org/10.1134/S0021364014090112
20. Y. Liu, H. Wang, J. Ho, R. C. Ng, et al., Nat. Commun. **10**, 1 (2019). https://doi.org/10.1038/s41467-019-12360-w
21. A. I. Maydykovskiy, E. A. Mamonov, N. V. Mitetelo, S. Soria, and T. V. Murzina, JETP Letters **115**, 261 (2022). https://doi.org/10.31857/S1234567822050044
22. M. Lyubomirskiy, F. Koch, K. A. Abrashitova, et al., Opt. Express. **27**, 8639 (2019). https://doi.org/10.1364/OE.27.008639
23. Y.-L. Zhang, Q.-D. Chen, H. Xia, and Ho.-B. Sun, Nano Today. **5**, 435 (2010). https://doi.org/10.1016/j.nantod.2010.08.007
24. V. F. Paz, M. Emons, K. Obata, et al., J. Laser Appl. **24**, 042004 (2012). https://doi.org/10.2351/1.4712151
25. Y.-H. Yu, Z.-N. Tian, T. Jiang, et al., Opt. Commun. **362**, 69 (2016). https://doi.org/10.1016/j.optcom.2015.08.039
26. M. I. Sharipova, T. G. Baluyan, K. A. Abrashitova, et al., Opt. Mater. Express **11**, 371 (2021). https://doi.org/10.1364/OME.416457
27. F. Seiboth, D. Brückner, M. Kahnt, et al., J. Synchrotron Radiat. **27**, 1121 (2020). https://doi.org/10.1107/S1600577520007900
28. A. Mikhaylov, S. Reich, M. Zakharova, et al., J. Synchrotron Radiat. **27**, 788 (2020). https://doi.org/10.1107/S1600577520002830
29. A. Kubec, M.-C. Zdora, U. T. Sanli, et al., Nat. Commun. **13**, 1 (2022). https://doi.org/10.1038/s41467-022-28902-8
30. A. Barannikov, M. Polikarpov, P. Ershov, et al., J. Synchrotron Radiat. **26**, 714 (2019). https://doi.org/10.1107/S1600577519001656
31. H.-B. Sun, K. Takada, M.-S. Kim, et al., Appl. Phys. Lett. **83**, 1104 (2003). https://doi.org/10.1063/1.1599968
32. L. Zheng, K. Kurselis, A. El-Tamer, et al., Nanoscale Res. Lett. **14**, 1 (2019). https://doi.org/10.1186/s11671-019-2955-5
33. A. V. Pisarenko, R. D. Zvagelsky, D. A. Kolymagin, et al., Optik. **201**, 163350 (2020). https://doi.org/10.1016/j.ijleo.2019.163350
34. M. Malinauskas, M. Farsari, A. Piskarskas, S. Juodkazis, Phys. Rep. **533**, 1 (2013). https://doi.org/10.1016/j.physrep.2013.07.005
35. A. Ovsianikov, J. Viertl, B. Chichkov, et al., ACS Nano. **2**, 2257 (2008). https://doi.org/10.1021/nn800451w
36. B. Lengeler, Ch.G. Schroer, M. Kuhlmann, et al., J. Phys. D: Appl. Phys. **38**, A218 (2005). https://doi.org/10.1088/0022-3727/38/10A/042